Multiphoton Resonance Meets Tunneling Ionization: High-Efficient Photoexcitation in Strong-Field-Dressed Ions

Yewei Chen,[1,3,*] Hongbin Lei,[2,*] Quanjun Wang,[1] Hongqiang Xie,[4] He Zhang,[1] Xu Lu,[1,5] Ning Zhang,[1,5] Shunlin Huang,[1] Yuzhu Wu,[1,6] Jianpeng Liu,[2] Qian Zhang,[2] Yi Liu,[3] Zengxiu Zhao,[2] Jing Zhao,[2,†] and Jinping Yao[1,‡]

[1]*State Key Laboratory of High Field Laser Physics, Shanghai Institute of Optics and Fine Mechanics, Chinese Academy of Sciences, Shanghai 201800, China*

[2]*Department of Physics, National University of Defense Technology, Changsha 410073, China*

[3]*School of Optical-Electrical and Computer Engineering, University of Shanghai for Science and Technology, Shanghai 200093, China*

[4]*School of Science, East China University of Technology, Nanchang 330013, China*

[5]*Center of Materials Science and Optoelectronics Engineering, University of Chinese Academy of Sciences, Beijing 100049, China*

[6]*School of Microelectronics, Shanghai University, Shanghai 200444, China*

(Received 3 July 2023; accepted 30 July 2024; published 13 September 2024)

Tunneling ionization, a fascinating quantum phenomenon, has played the key role in the development of attosecond physics. Upon absorption of a few tens of photons, tunneling ionization creates ions in different excited states and even enables the formation of population inversion between ionic states. However, the underlying physics is still being debated. Here, we demonstrate a significant enhancement in the efficiency of multiphoton excitation when ionization of neutral molecules and resonant excitation of ions coexist in strong laser fields. It facilitates the dramatic increase in population inversion and lasing radiation in N_2^+ around 1000 nm pump wavelength. Utilizing the ionization-coupling theory, we discover that the synergistic interplay between tunneling ionization and multiphoton excitation enables the ionic coherence to be maximized by phase locking of the periodically created ionic dipoles and consistently maintain an optimal phase for the follow-up photoexcitation. This Letter provides new insights into the photoexcitation mechanism of ions in strong laser fields and opens up a route for optimizing ionic lasing radiations.

DOI: 10.1103/PhysRevLett.133.113201

Photoexcitation and photoionization are the well-known fundamental processes of laser-matter interaction. Photoexcitation mainly involves transitions of electrons from ground states to excited states, while photoionization leads to the breakdown of atoms with electrons ejected. In most cases, they are regarded as two independent processes and manipulated separately by adjusting laser parameters. However, in the strong-field regime, the outermost electrons readily escape from the distorted potential barrier at the instant of light field oscillation [1], leading to the creation of extreme nonstationary ionic states that trigger attosecond correlated electron-hole dynamics [2–4]. Along with tunnel ionization, photoexcitation of ions also probably takes place and plays an important role. The relevant investigations on the quantum many-body systems have aroused extensive interest in the past few decades [5–11].

Recently, some studies have demonstrated the interplay of strong-field ionization and excitation. Sabbar *et al.* revealed the influence of polarization on the attosecond dynamics of tunneling ionization with a few-cycle laser pulse [12]. Zhang *et al.* demonstrated that the instantaneous ionization injection enhances the ionic excited-state population [13]. The combination of strong-field ionization and multiphoton processes can even change the optical radiation properties of bound-bound transitions [14]. Moreover, recent studies on N_2^+ lasing mechanisms indicate the ionic photoexcitation is indispensable for inducing a net optical gain [13,15–18], since the ionization alone hardly induces population inversion in the ionic system [19,20]. Very recently, Yuen *et al.* studied the contribution of tunneling ionization coherence to single ionization and sequential double ionization [21]. All these studies confirm that tunneling ionization and photoexcitation cannot be considered independently.

In this Letter, we study the joint contribution of tunneling ionization and multiphoton resonant excitation to the ionic population redistribution by measuring N_2^+ lasing as a function of pump wavelengths. The experimental and theoretical results substantialize that the population in the ionic excited state reaches maximum around the 1000 nm

*These authors contributed equally to this work.

†Contact author: jzhao@nudt.edu.cn

‡Contact author: jinpingmrg@163.com

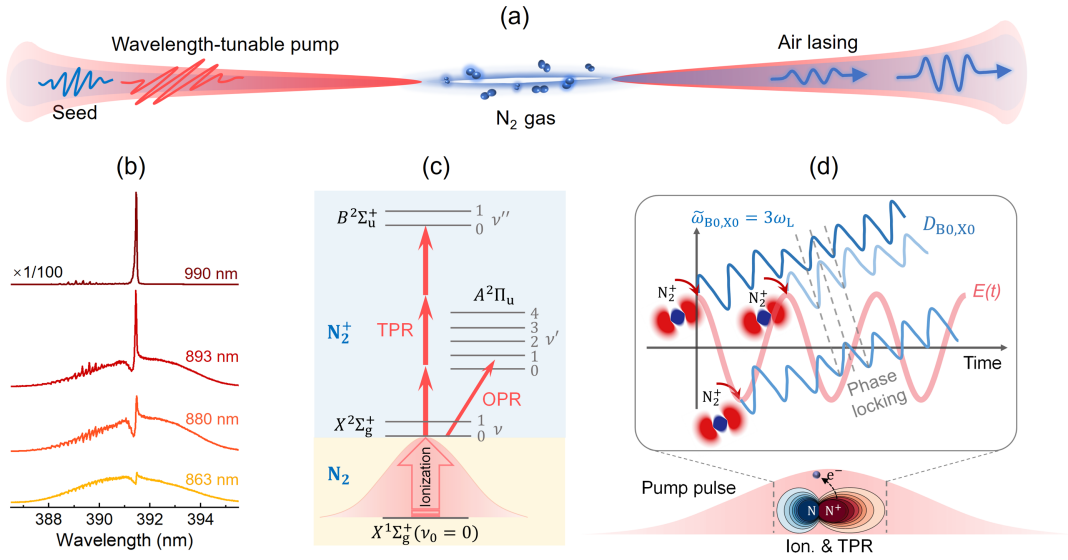

FIG. 1. (a) Schematic of the experiment setup. (b) The typical emission spectra measured at different pump wavelengths. (c) Energy-level diagram used to describe ionization and photoexcitation in a strong laser field. (d) Schematic illustration of physical mechanism of high-efficient photoexcitation in the strong-field-dressed ions when tunnel ionization and TPR coexist.

wavelength. We reveal that the high-efficient excitation at the optimal wavelength is the result of synergistic interplay between tunneling ionization and photoexcitation. The periodic ionization injection at the peaks of the oscillating electric field induces ionic dipoles periodically and endows them with the optimal phase for photoexcitation. The resonance of the pump laser with field-dressed ionic states enables the optimal buildup of ionic coherence due to phase locking and constructive interference of dipoles born at different moments. Therefore, compared with the individual contribution of ionization or multiphoton excitation, the ionic excited-state population is enhanced by nearly 1 order of magnitude when the two effects coexist.

Compared with previous studies [12–18,21], this Letter emphasizes the crucial role of ionic coherence and phase matching between the ionic dipole and the driver laser in the photoexcitation, and further reveals the interplay of tunneling ionization and multiphoton resonance by the subcycle dipole phase analysis. Moreover, the tunnel ionization restricts the ionic photoexcitation starting near the pump pulse peak. Such an ionization gate further promotes excitation efficiency, and manifests uniqueness of the strong-field-dressed ionic system. Three-photon Rabi oscillation takes places in such a quantum system, which has been rarely reported. This Letter sheds new light on multiphoton excitation in strong laser fields, and provides critical guidance for optimizing ionic lasing and extending its applications.

The experiments were performed with a wavelength-tunable pump pulse and an external seed pulse, as shown in Fig. 1(a). The pump pulse with a tunable wavelength from 850 to 1070 nm was generated by frequency doubling of the idler beam from an optical parametric amplifier. The seed pulse was provided by frequency doubling of the 800 nm laser. The pump and seed beams with the perpendicular polarization were combined by a dichroic mirror and then were collinearly focused into the nitrogen gas chamber using an $f = 10$ cm lens. The pump energy was measured before the dichroic mirror with nearly the same transmission at different pump wavelengths. The pump intensity was calculated with the assumption of linear propagation, which is overestimated due to the neglected plasma defocusing and transmission loss. The pump-seed delay was individually optimized in different pumping conditions, ensuring generation of the strongest N_2^+ lasing at each pump wavelength. After filtering, the signal was fully collected into a spectrometer, and a polarizer was used to suppress the signal produced by the pump alone.

Experimentally, the focused intensities of pump lasers at various wavelengths were kept nearly the same by controlling the incident energy, according to the measured pulse durations and focused radii. As illustrated in Fig. 1(b), the spectral lineshapes of seed pulses vary from absorption to strong emission while tuning the pump wavelength. The seed pulse is significantly amplified at the 990 nm pump wavelength, giving rise to strong N_2^+ lasing radiation at 391.4 nm, which is ascribed to the transition between $B^2\Sigma_u^+(\nu'' = 0)$ and $X^2\Sigma_g^+(\nu = 0)$ of N_2^+. Figure 1(c) shows the corresponding tunnel ionization and photoexcitation processes in the optimal pumping condition. Along with the tunnel ionization, one-photon resonance (OPR) and three-photon resonance (TPR) occur among the strong-field-dressed ionic states, resulting in high-efficient photoexcitation. The physical mechanism is shown in Fig. 1(d) and will be discussed later. As seen in Fig. 1(b), remarkable Fano lineshapes appear at some

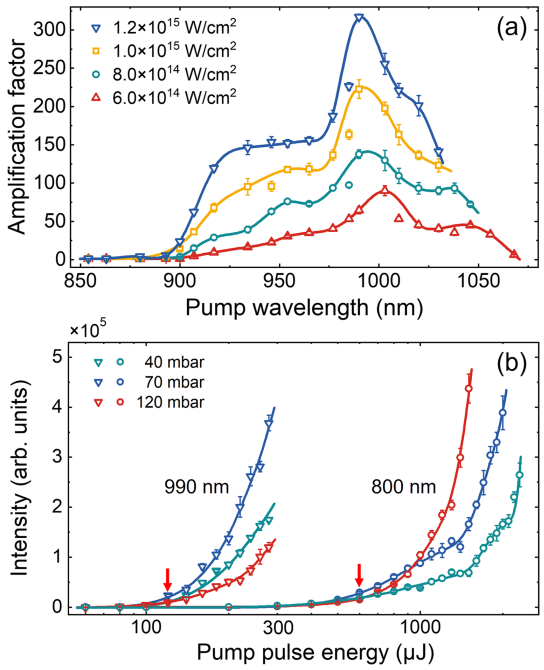

FIG. 2. (a) The amplification factor of seed pulses in the 40-mbar nitrogen gas as a function of the pump wavelength at different intensities. (b) The dependence of N_2^+ lasing pumped by the 800 nm and 990 nm lasers on the pump energy. Solid curves are numerical fits of experimental data to guide the eyes.

wavelengths, which arise from the interference between the seed pulse and seed-stimulated N_2^+ lasing radiation. Since the pump pulse does not introduce an additional phase to the lasing radiation, only the relative strength between N_2^+ lasing and the seed changes with the pump wavelength. Thus, the Fano lineshape becomes asymmetric with the enhanced N_2^+ lasing. These results indicate that the population distribution in the two ionic states strongly depends on the pump wavelength.

To characterize the amplification capability of N_2^+ prepared by different pump lasers, we investigated the amplification factor, defined as the ratio of the spectral intensity of N_2^+ lasing to that of the seed at the 391.4 nm wavelength, as a function of pump wavelength. As shown in Fig. 2(a), amplification was observed over a broad range, and the amplification factor gradually increases with the pump intensity. For all measured intensities, the maximum gain appears near 1000 nm. When the intensity increases from 6×10^{14} W/cm^2 to 8×10^{14} W/cm^2, the optimal wavelength shifts from 1003 nm to 990 nm. However, it remains constant with further increasing intensity. The amplification factor exceeding 300 is experimentally achieved in the 990 nm, 1.2×10^{15} W/cm^2 pumping case.

In previous studies, the 800 nm laser was commonly utilized to study N_2^+ lasing [15–17,22–25]. Figure 2(b) shows the dependence of N_2^+ lasing intensity on the pump energy in the 990 nm and 800 nm pumping cases when the gas pressures were 40, 70, and 120 mbar. Considering the spatial difference of incident 800 nm and 990 nm lasers, the 800 nm laser was focused by an $f = 15$ cm lens to ensure nearly the same focal spot with that of the 990 nm laser. We can clearly see that N_2^+ lasing begins to grow rapidly around the energy of 120 μJ for the 990 nm pumping, while the significant increase occurs near 600 μJ for the 800 nm pumping, as indicated by red arrows. Thus, the lasing threshold with the 990 nm pump laser is merely 1/5 of that with the 800 nm laser. At the gas pressure of 70 mbar, the seed is amplified by nearly 400 times in the 990 nm, 280 μJ pumping case, whereas the gain has not been established by the 800 nm laser with the comparable energy. These results demonstrate obvious advantages of the 990 nm pumping.

To interpret the experimental results, we simulate N_2^+ population with the ionization-coupling model [13,14],

$$\frac{d\rho^+}{dt} = -i[H(t), \rho^+] + \left(\frac{d\rho^+_{n\nu}}{dt}\right)_{\text{ionize}} + \left(\frac{d\rho^+_{n\nu,n'\nu'}}{dt}\right)_{\text{decay}}. \quad (1)$$

Here, ρ^+ denotes the density matrix of N_2^+, and $H(t)$ is the Hamiltonian, $n(n')$ represents $X^2\Sigma_g^+$, $A^2\Pi_u$ and $B^2\Sigma_u^+$ states (abbreviated as X, A, and B), and $\nu(\nu')$ represents vibrational states ($\nu, \nu' = 0 \sim 4$). The terms on the right side of Eq. (1) sequentially represent the laser-ion coupling, transient ionization injection, and decay process, respectively. To mimic experimental conditions, we set the pulse duration to 60 fs and the dephasing time to 1 ps for all transitions in the simulations, and assume the angle between the molecular axis and the laser field as 45°.

The intensity of seed-amplified lasing at 391.4 nm is mainly determined by the population difference between $B(\nu'' = 0)$ and $X(\nu = 0)$, i.e., $\Delta n = \rho^+_{B0,B0} - \rho^+_{X0,X0}$. Figure 3(a) shows the calculated Δn as functions of the pump wavelength and intensity. The maximum gain appears near 1000 nm. In the strong-gain region, Δn is strongly modulated with the change of pump laser parameters, and its value depends on the end phase φ of the three-photon Rabi oscillation. Thus, three gain channels basically match with the results of three-photon Rabi oscillation, as indicated by red, magenta, and blue lines [26]. It actually arises from TPR of the pump laser with the field-dressed $B(\nu'' = 0) - X(\nu = 0)$ transition, i.e., $\tilde{\omega}_{B0,X0} = 3\omega_L$, where $\tilde{\omega}_{B0,X0}$ is the cycle-averaged maximum transition energy and ω_L is the pump laser frequency. Multiphoton Rabi oscillation is rarely explored as it is much weaker than one-photon Rabi oscillation [29,30]. Ions can withstand stronger lasers than neutral molecules, thereby enabling the study of multiphoton Rabi oscillations.

Figure 3(b) represents the quantitative relation between Δn and the pump wavelength. It can be seen that the population inversion begins to appear near 1050 nm at the intensity of 1.5×10^{14} W/cm^2, and then gradually extends to shorter wavelengths as the pump intensity increases.

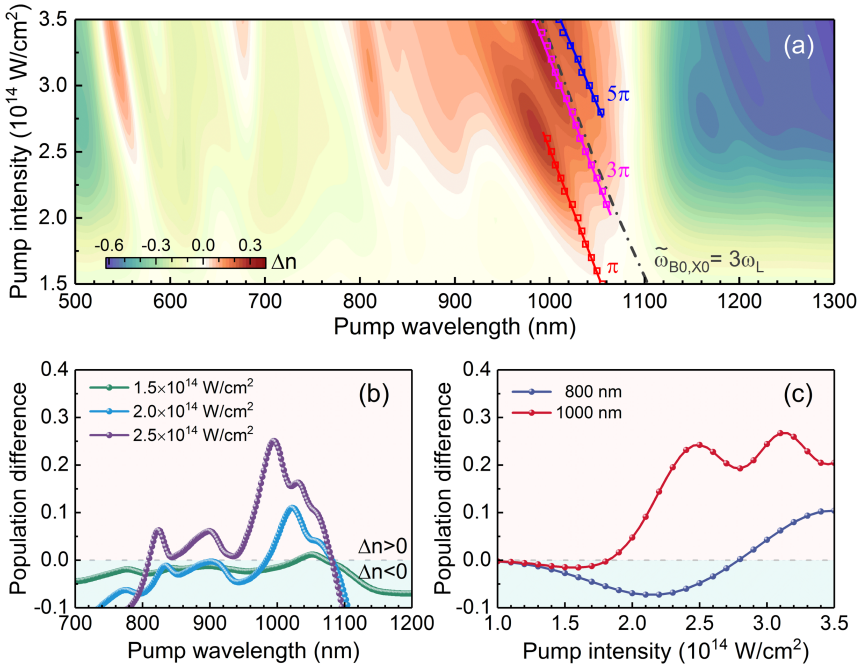

FIG. 3. (a) The calculated population difference between $B(\nu''=0)$ and $X(\nu=0)$ states as functions of the pump wavelength and intensity. The red, magenta, and blue lines indicate the three-photon Rabi oscillation ending at $\varphi=\pi$, 3π, and 5π, respectively. Black dash-dot line indicates the gain channel of TPR given by $\tilde{\omega}_{B0,X0}=3\omega_L$. (b) The population difference versus the pump wavelength at three typical pump intensities. (c) The dependence of population difference on the intensity for the 800 nm and 1000 nm pumping cases.

When the intensity reaches 2.5×10^{14} W/cm^2, population inversion can be established in a broad range, with a gain peak appearing near 1000 nm. Numerical calculations are in reasonable agreement with experimental results, although there are quantitative differences. Figure 3(c) compares the pump-intensity dependences of Δn for the 800 nm and 1000 nm pumping cases. The pump intensity required for population inversion is much lower for the 1000 nm pumping, which well explains the experimental observations in Fig. 2(b). It is noteworthy that although the simulation results shown in Fig. 3 do not include the ionic rotation, they still reproduce the main features of experimental results. We also performed simulations with the model including rotation, and obtained similar results [26], suggesting that the ionic rotation is not important here compared with previous studies [31,32]. In addition, propagation effects are not considered theoretically, which could be the main reason for the quantitative differences between theoretical and experimental results. Experimentally, the influence has been minimized by ensuring similar focal volumes of various wavelengths and choosing relatively low pressures.

To uncover the physical mechanism of enhanced population inversion near 1000 nm, we further calculated the state-resolved population as a function of the pump wavelength at the intensity of 2.5×10^{14} W/cm^2. As shown in Fig. 4(a), the population in $X(\nu=0)$ state decreases significantly over a broad pump wavelength range, which can be attributed to OPR excitation from $X(\nu=0)$ to multiple vibrational levels of A state [26]. In addition, the population in $B(\nu''=0)$ state shows a pronounced peak around 1000 nm, which approximately matches with the three-photon Rabi oscillation. Surprisingly, TPR excitation is very efficient and even prevails over OPR excitation from $X(\nu=0)$ to $A(\nu'=0)$ around the TPR wavelength.

To gain a deeper understanding for high-efficient TPR excitation, we compared the population evolution of the $B(\nu''=0)$ state in four cases, i.e., considering only ionization, only TPR, and ionization-coupling (IC) with or without TPR. The 800 nm laser is used for the case of IC without TPR, whereas the 983 nm laser is used for other cases. As illustrated in Fig. 4(b), when merely considering ionization or TPR, only 3.2% and 0.7% ions are excited to $B(\nu''=0)$ state, respectively. The simultaneous involvement of ionization and coupling substantially improves the population of $B(\nu''=0)$ (blue line) due to ionic instantaneous polarization [13]. The TPR and ionization injection coexist at the 983 nm wavelength. In this case, the population of $B(\nu''=0)$ continually grows within the laser field and finally reaches 32.2% (red line), which is nearly 1 order of magnitude higher compared with the case considering only TPR or only ionization. These results indicate that high-efficient excitation originates from the interplay of ionization injection and TPR.

To elucidate the interplay of the two effects, we analyzed the phase matching between the ionic dipole $D_{B0,X0}$ and the laser field $E(t)$ in Fig. 5. Since the excitation rate is proportional to $\mathrm{Im}(D_{B0,X0})E(t)$ [33], the phase matching

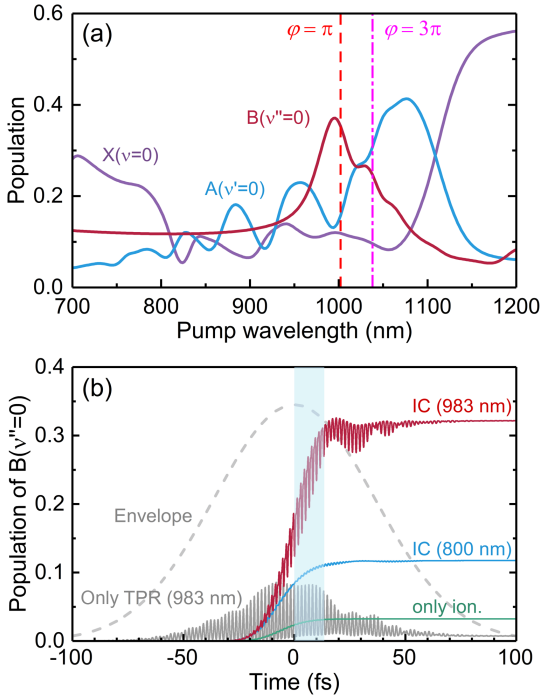

FIG. 4. (a) The population in $X(\nu=0)$, $A(\nu'=0)$, and $B(\nu''=0)$ states as a function of the pump wavelength. The red dashed line and magenta dash-dot line indicate the three-photon Rabi oscillation ending at $\varphi=\pi$ and 3π, respectively. (b) The population evolution of the $B(\nu''=0)$ state in different cases. The dashed line denotes the electric field envelope. The shaded region indicates the time window of phase analysis in Fig. 5.

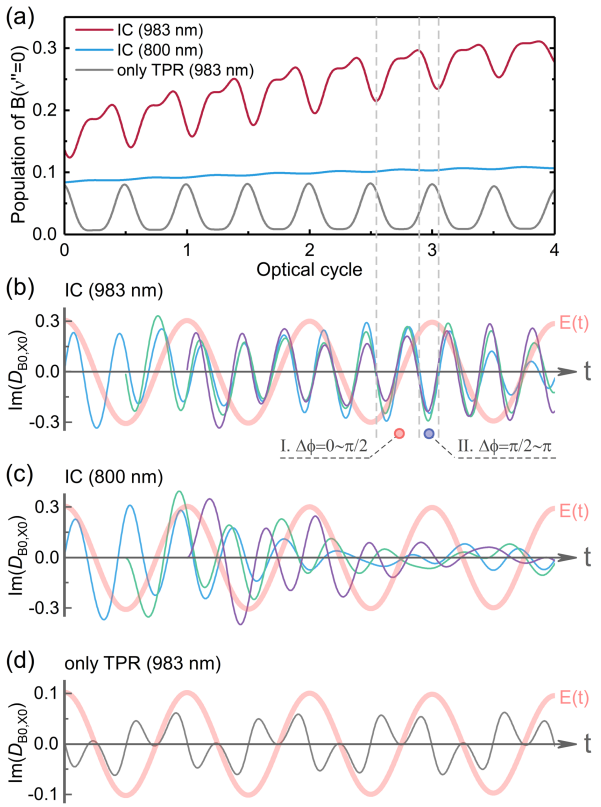

FIG. 5. (a) The calculated population dynamics of the $B(\nu''=0)$ state. The evolution of ionic dipoles created at different moments at the pump wavelength of (b) 983 nm and (c) 800 nm when the ionization injection is included. For comparison, the result in the only TPR case is shown in (d).

between them determines the photoexcitation efficiency and direction of population transfer. When the phase difference $\Delta\phi$ falls in the region of $[0,\pi/2]$, N_2^+ will be pumped to the excited state. For the case of $\Delta\phi\in[\pi/2,\pi]$, the opposite transition occurs.

We first compare the evolution of ionic dipoles in the 983 nm and 800 nm pumping cases to clarify the contribution of TPR, as shown in Figs. 5(b) and (c). Along with the periodic injection of ions, the ionic dipoles are periodically created, as shown by the blue, green, and purple curves. When TPR coexists with ionization injection, the dipoles born at different instants possess the same phase. The phase locking not only facilitates the optimal buildup of ionic coherence, but also provides it the optimal phase for the photoexcitation from $X(\nu=0)$ to $B(\nu''=0)$, which can be understood by the phase analysis in Fig. 5(b). In region I, $\Delta\phi$ mainly varies in the $0\sim\pi/2$ range, enabling the increase of excited-state population. In region II, the contrary process occurs. Since in-phase oscillation of $\mathrm{Im}(D_{\mathrm{B0,X0}})$ and $E(t)$ lasts for longer time, the excitation is always more efficient than the de-excitation, enabling the net increase of excited-state population within each half period. At the 983 nm wavelength, the phase locking can remain nearly ten cycles. The large ionic dipole carrying the optimal phase leads to continuous growth of population in $B(\nu''=0)$ state, as illustrated by the red curve in Fig. 5(a). At the 800 nm wavelength, the ionic dipoles created at different moments exhibit random phases due to the absence of TPR, as illustrated in Fig. 5(c). In this case, the ionic coherence cannot be efficiently established and maintain the optimal phase with the driving laser, thereby rendering the photoexcitation less efficient.

The ionization injection is also crucial for promoting ionic excitation. If only TPR is considered, as illustrated in Fig. 5(d), the induced ionic dipole has accumulated a certain phase when the TPR takes place, making it difficult to own an optimal phase for photoexcitation. The comparative analysis indicates that the cooperation of tunneling ionization and multiphoton resonance greatly enhances the ionic excited-state population. It can be attributed to optimal buildup of ionic coherence and phase matching of the ionic dipole and the driver laser. The physical mechanism is briefly illustrated in Fig. 1(d). Moreover, the highly nonlinear dependence of tunneling ionization on the laser field strength helps the photoexcitation truncate the strong and slowly varying laser field, which is beneficial to improve the efficiency of TPR. These effects rarely take place in neutral atoms or molecules, thus showing advantages of ionic system prepared by strong laser fields.

In summary, we experimentally demonstrated that the optical gain can be achieved in N_2^+ across a broad range of pump wavelengths, while the maximum gain is located near 1000 nm rather than 800 nm. The theoretical simulation reproduces experimental results, and reveals that the enhanced population inversion is attributed to the synergistic interplay of ionization injection and three-photon resonance. Their simultaneous involvement makes the ionic excited-state population be nearly 1 order of magnitude higher compared to their individual contribution. The subcycle analysis on ionic dipoles shows that when multiphoton resonance meets tunneling ionization, ionic coherence is maximized by phase locking of the periodically created ionic dipoles, and carries an optimal phase for follow-up photoexcitation. The optimal buildup of ionic coherence facilitates continuous, high-efficient population transfer from the ionic ground state to the excited state. This work uncovers a new photoexcitation mechanism, which is universal for ionic systems prepared by strong laser fields. The high-efficient excitation scheme opens up great opportunities for generating air lasing by using compact fiber lasers due to the dramatic decrease of lasing threshold.

Acknowledgments—This work is supported by the National Natural Science Foundation of China (Grants No. 12034013, No. 12234020, No. 12274428, No. 12074063, No. 12264003), Project of Chinese Academy of Sciences for Young Scientists in Basic Research (Grant No. YSBR-042), Youth Innovation Promotion Association of Chinese Academy of Sciences (Grant No. Y2022072), and Natural Science Foundation of Shanghai (Grants No. 22ZR1481600, No. 23ZR1471700).

[1] L. V. Keldysh, Sov. Phys. JETP **20**, 1307 (1965).
[2] E. Goulielmakis, Z. H. Loh, A. Wirth, R. Santra, N. Rohringer, V. S. Yakovlev, S. Zherebtsov, T. Pfeifer, A. M. Azzeer, M. F. Kling, S. R. Leone, and F. Krausz, Nature (London) **466**, 739 (2010).
[3] P. M. Kraus, B. Mignolet, D. Baykusheva, A. Rupenyan, L. Horný, E. F. Penka, G. Grassi, O. I. Tolstikhin, J. Schneider, F. Jensen, L. B. Madsen, A. D. Bandrauk, F. Remacle, and H. J. Wörner, Science **350**, 790 (2015).
[4] N. V. Golubev, J. Vaníček, and A. I. Kuleff, Phys. Rev. Lett. **127**, 123001 (2021).
[5] D. N. Fittinghoff, P. R. Bolton, B. Chang, and K. C. Kulander, Phys. Rev. Lett. **69**, 2642 (1992).
[6] O. Smirnova, Y. Mairesse, S. Patchkovskii, N. Dudovich, D. Villeneuve, P. Corkum, and M. Y. Ivanov, Nature (London) **460**, 972 (2009).
[7] C. Ott, A. Kaldun, L. Argenti, P. Raith, K. Meyer, M. Laux, Y. Zhang, A. Blättermann, S. Hagstotz, T. Ding, R. Heck, J. Madroñero, F. Martín, and T. Pfeifer, Nature (London) **516**, 374 (2014).
[8] M. Vacher, M. J. Bearpark, M. A. Robb, and J. P. Malhado, Phys. Rev. Lett. **118**, 083001 (2017).
[9] R. E. F. Silva, I. V. Blinov, A. N. Rubtsov, O. Smirnova, and M. Ivanov, Nat. Photonics **12**, 266 (2018).
[10] J. Yao, W. Chu, Z. Liu, J. Chen, B. Xu, and Y. Cheng, Appl. Phys. B **124**, 73 (2018).
[11] Y. Huang, J. Zhao, Z. Shu, Y. Zhu, J. Liu, W. Dong, X. Wang, Z. Lü, D. Zhang, J. Yuan, J. Chen, and Z. Zhao, Ultrafast Sci. **2021**, 9837107 (2021).
[12] M. Sabbar, H. Timmers, Y.-J. Chen, A. K. Pymer, Z.-H. Loh, Scott G. Sayres, S. Pabst, R. Santra, and S. R. Leone, Nat. Phys. **13**, 472 (2017).
[13] Q. Zhang, H. Xie, G. Li, X. Wang, H. Lei, J. Zhao, Z. Chen, J. Yao, Y. Cheng, and Z. Zhao, Commun. Phys. **3**, 50 (2020).
[14] H. Lei, J. Yao, J. Zhao, H. Xie, F. Zhang, H. Zhang, N. Zhang, G. Li, Q. Zhang, X. Wang, Y. Yang, L. Yuan, Y. Cheng, and Z. Zhao, Nat. Commun. **13**, 4080 (2022).
[15] H. Xu, E. Lötstedt, A. Iwasaki, and K. Yamanouchi, Nat. Commun. **6**, 8347 (2015).
[16] J. Yao, S. Jiang, W. Chu, B. Zeng, C. Wu, R. Lu, Z. Li, H. Xie, G. Li, C. Yu, Z. Wang, H. Jiang, Q. Gong, and Y. Cheng, Phys. Rev. Lett. **116**, 143007 (2016).
[17] H. Li, M. Hou, H. Zang, Y. Fu, E. Lötstedt, T. Ando, A. Iwasaki, K. Yamanouchi, and H. Xu, Phys. Rev. Lett. **122**, 013202 (2019).
[18] V. T. Tikhonchuk, Y. Liu, R. Danylo, A. Houard, and A. Mysyrowicz, New J. Phys. **23**, 023035 (2021).
[19] M. V. Ammosov, N. B. Delone, and V. P. Kraĭnov, Sov. Phys. JETP **64**, 1191 (1986).
[20] X. M. Tong, Z. X. Zhao, and C. D. Lin, Phys. Rev. A **66**, 033402 (2002).
[21] C. H. Yuen and C. D. Lin, Phys. Rev. A **108**, 023123 (2023).
[22] J. Yao, G. Li, C. Jing, B. Zeng, W. Chu, J. Ni, H. Zhang, H. Xie, C. Zhang, H. Li, H. Xu, S. L. Chin, Y. Cheng, and Z. Xu, New J. Phys. **15**, 023046 (2013).
[23] Y. Liu, P. Ding, G. Lambert, A. Houard, V. Tikhonchuk, and A. Mysyrowicz, Phys. Rev. Lett. **115**, 133203 (2015).
[24] M. Britton, P. Laferrière, D. H. Ko, Z. Li, F. Kong, G. Brown, A. Naumov, C. Zhang, L. Arissian, and P. B. Corkum, Phys. Rev. Lett. **120**, 133208 (2018).
[25] W. Zheng, Z. Miao, L. Zhang, Y. Wang, C. Dai, A. Zhang, H. Jiang, Q. Gong, and C. Wu, J. Phys. Chem. Lett. **10**, 6598 (2019).
[26] See Supplemental Material, which includes Refs. [27–29], at http://link.aps.org/supplemental/10.1103/PhysRevLett.133.113201 for the details of the influence of ionic rotation on population difference, population modulation induced by three-photon Rabi oscillation, and vibrational-resolved population of three electronic states.
[27] P. Marquetand, T. Weinacht, T. Rozgonyi, J. González-Vázquez, D. Geißler, and L. González. *Advances in Multi-Photon Processes and Spectroscopy* (World Scientific, Singapore, 2013), Vol. 21.
[28] P. L. Knight and P. W. Milonni, Phys. Rep. **66**, 21 (1980).
[29] P. W. Milonni and J. H. Eberly, J. Chem. Phys. **68**, 1602 (1978).
[30] M. Fushitani, C. N. Liu, A. Matsuda, T. Endo, Y. Toida, M. Nagasono, T. Togashi, M. Yabashi, T. Ishikawa,

Y. Hikosaka, T. Morishita, and A. Hishikawa, Nat. Photonics **10**, 102 (2016).
[31] M. Richter, M. Lytova, F. Morales, S. Haessler, O. Smirnova, M. Spanner, and M. Ivanov, Optica **7**, 586 (2020).
[32] Y. Zhang, E. Lötstedt, and K. Yamanouchi, Phys. Rev. A **101**, 053412 (2020).
[33] P. Meystre and M. Sargent, *Elements of Quantum Optics* (Springer-Verlag, Heidelberg, 1998).